4ICEGE
Thessaloniki-GREECE 2007

4th International Conference on
Earthquake Geotechnical Engineering
June 25-28, 2007
Paper No. 1538

VARIATION OF RECORDED AND SIMULATED NEAR-FAULT GROUND MOTION FROM THE 2004 PARKFIELD, CALIFORNIA EARTHQUAKE

Arben PITARKA [1] and Nancy COLLINS [2]

ABSTRACT

The 2004 Parkfield earthquake is one of the best-recorded earthquakes in California. The most striking characteristic of the near-fault ground motion from the 2004 Parkfield earthquake is its large variability in terms of peak acceleration, peak velocity and duration. We developed kinematic and dynamic rupture models of the earthquake using near-fault ground motions, and also estimated site effects using weak-motion records from a local earthquake. In order to investigate the implication of the rupture kinematics and dynamics, and local site effects in the amplitude and spatial variation of the near-fault ground motion we performed analyses of recorded and synthetic broadband time histories of acceleration simulated using both kinematic and dynamic rupture models. Our analyses suggest that site effects, including fault zone effects, caused much of the observed amplification and deamplification of the ground motion and that they were the primary factors in producing very variable near-fault ground motion.

Keywords: Strong Ground Motion, Site Effects, Earthquake Rupture, Ground Motion Simulation

INTRODUCTION

The M6.0 2004 Parkfield earthquake occurred on a right lateral segment of the San Andreas fault. The San Andreas fault forms the boundary between the granitic Salinian block on the west and Southern Diablo Range with sedimentary Franciscan terrane on the east. Based on the distribution of aftershocks that occurred immediately after the earthquake the fault length and width were estimated to be 35km and 15 km, respectively (Hardebeck and Michael, 2004). No co-seismic surface rupture appeared, but surface slip began several hours after the main shock (Langbein et al., 2005). The fault plane is almost vertical and has a strike angle of 140^{o} (Thurber et al.,2006). The shallow underground structure is characterized by velocity contrast across the fault, with the northeast side about 20% slower in the top 10 km. Below 10 km the velocity contrast gradually diminishes with depth.

The earthquake was recorded by a large number of strong motion stations. In this study we investigated ground motion records from 47 CGC (California Gelogical Survey) and 11 USGS (United States Geological Survey) strong motion stations. With the objective of explaining the main features of the recorded near-fault motion we performed analyses of the source process and site effects using both recorded and simulated broad-band ground-motion time histories.

[1] URS Corporation, Pasadena, California, Email: arben_pitarka@urscorp.com
[2] URS Corporation, Pasadena, California

NEAR-FAULT GROUND MOTION CHARACTERISTICS

Figure 1 shows the map of the Parkfield area and location of CGC and USGS strong motion stations used in this study. A typical example of very variable near-fault ground motion recorded during the earthquake is shown in Figure 2. In this figure we have displayed the fault-normal component of two selected acceleration time histories and their spectrogram recorded at stations PF14 and PF15 located near the northern end of the fault. Because of the complex shallow fault geometry it is not certain whether these two stations are on the same side of the fault. The ground motion recoded at these two stations is very different even though the distance between the two stations is only 3.5 km. The 1.3 g peak ground acceleration recorded at station PF14 is the second highest recorded during the Parkfield earthquake (Shakal et al., 2005). The acceleration time history at this station has a relatively short duration and is dominated by two large pulses originated at the source. The pulses are energetic at a very narrow frequency band between 1Hz and 3Hz (see Figure 2). In contract, the acceleration time history at station PF15 has a much smaller amplitude and longer duration. At this station many large amplitude phases have distinct frequency contents that are centered at 1Hz, 2.5 Hz and 5Hz, respectively. The coda waves are mainly composed of small amplitude pulses of 1 sec duration.

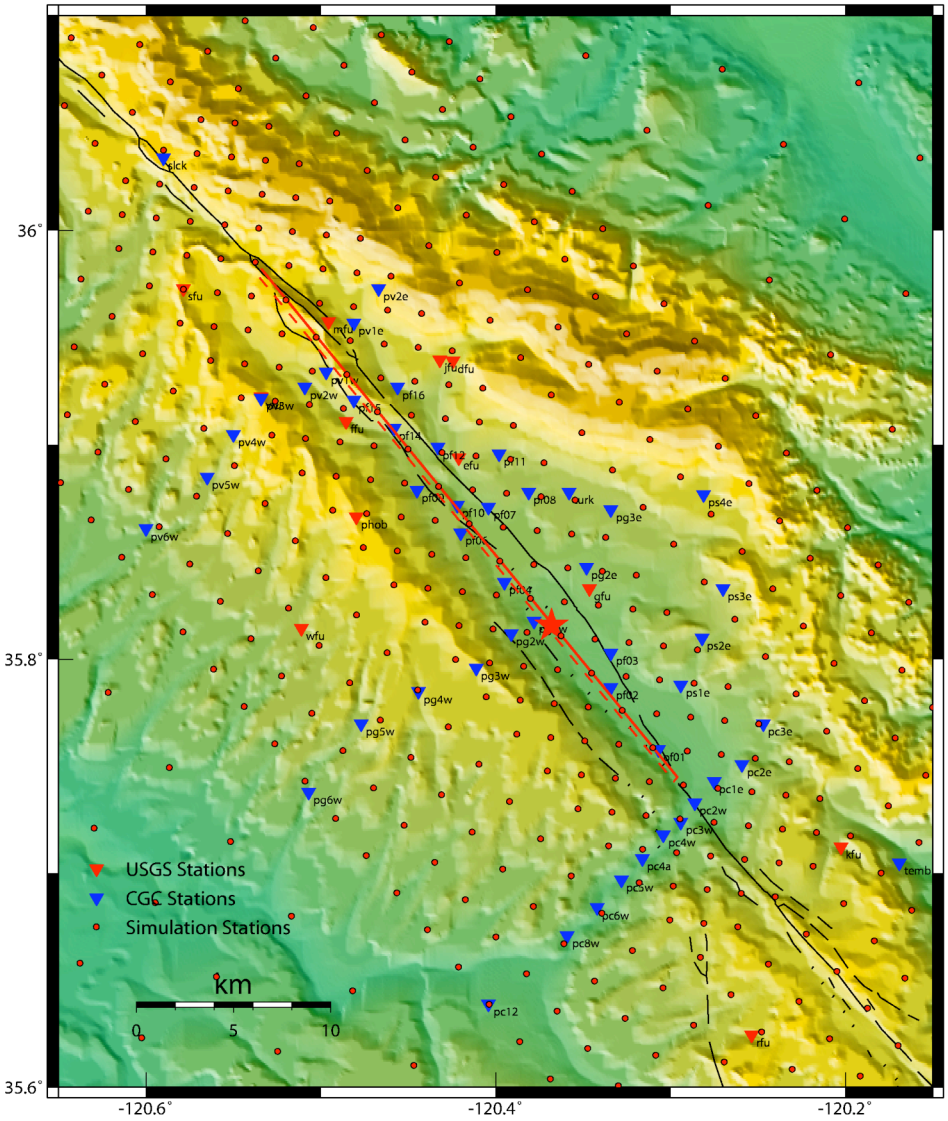

Figure 1. Map of the Parkfield area showing the faults trace (red line), the epicenter of the 2004 Parkfield earthquake (star) and CGC and USGS strong motion station locations. Red dots show the location of sites used in mapping simulated ground motion.

Such striking dissimilarities between neighboring stations were only observed at regions near the fault trace. They are indications of fault zone effects which mainly suppress the amplitude of high frequency motion and increase the duration of the ground motion.

In Figures3a and 3b we compare the recorded peak acceleration and that predicted by the empirical attenuation model of Abrahamson and Silva (1997), for both fault-normal and fault-parallel components. The comparison indicates that the stations that recorded peak ground motion acceleration below the expected value are all located within less than 1 km from the fault, probably in the fault zone. In contrast, stations with higher than expected acceleration are clustered at fault distances between 2-4 km. At longer distances the recorded ground motion is slightly smaller than that predicted by the attenuation model at all analyzed frequencies. The generally low-level of the observed ground motion can be explained by the fact that this was a low stress drop event. The difference between fault-normal and fault-parallel components remains significant up to at least 3.3Hz. This suggests that the rupture directivity for strike-slip event remains effective even at high frequencies.

These general features of recorded data indicate that the widely observed variable near-fault motion may have been caused by factors other than source effects. Such factors include fault zone effects and local site effects. Studies of fault-zone trapped waves have delineated a 150 m-wide fault zone characterized by low velocity and cracked rock (Li et al., 2006; Peng et al.,2003; Thurber et al., 2003). The width of the fault zone and that of damaged rock may vary along the fault. During the rupture the fault zone weakens the high-frequency motion generated at the crack tip while it amplifies waves trapped within the fault zone. As it will be shown below, our study does not rule out the possibility of increased ground motion due to local source rupture effects in some small areas near the north end of the fault. In the fault segment near these areas our rupture dynamics model shows small patches of larger stress-drop.

LOCAL SITE EFFECTS

We used the recoded motion from the 1983 M_w6.5 Coalinga earthquake to estimate the elastic local site response at Parkfield array stations that recorded both earthquakes. The stations used in analyses of local site effects are shown in Figure 4. The Coalinga earthquake occurred about 30 km NE of the epicenter of the Parkfield earthquake (Eberhart-Phillips, 1989). Based on the large epicentral distance from the array, we assumed that the incoming motion from the source of the Coalinga earthquake was the same at all Parkfield stations. The site effect was calculated as the ratio between the smoothed amplitude spectrum of recorded motion at each station and the reference spectrum calculated as the log average of all smoothed spectra. In order to reduce possible discrepancies due to the velocity contrast in the fault region the reference spectrum was calculated separately for stations on the east and west side of the fault. The calculated spectral ratio at a given frequency was considered as the local amplification factor.

The amplification factors estimated at frequencies 0.5Hz, 1Hz, 3Hz, 8Hz, 12Hz and 25 Hz are shown in Figure 5. In this figure closed blue circles correspond to amplitude ratios larger than 1, indicating amplification, and green circles correspond to amplitude ratios smaller than 1, indicating deamplification. A circle's radius is proportional to the corresponding amplification factor. The biggest site amplification of 3.6 is observed at 1Hz at station PF14. The broad-band amplification at this site indicates that the site effects have amplified the ground motion on a broad frequency range. Based on this result we concluded that the very high acceleration observed at this station is mainly due to site effects. This is also supported by another study of local site effects at station PF14 and nearby sites (Haddadi et al., 2006). According to their investigation at station PF14, station PF16, located near station PF14, and the surrounding sites the ground motions from several earthquakes, including two aftershocks of the 2004 Parkfield earthquake, 1983 M6.5 Coalinga earthquake and M6.0 San Simeon

earthquake, are characterized by elevated amplitudes. They also concluded that during the 2004 Parkfield earthquake the peak ground acceleration at station PF16 at which the ground motion record was clipped, the peak acceleration may have exceeded 2.5g.

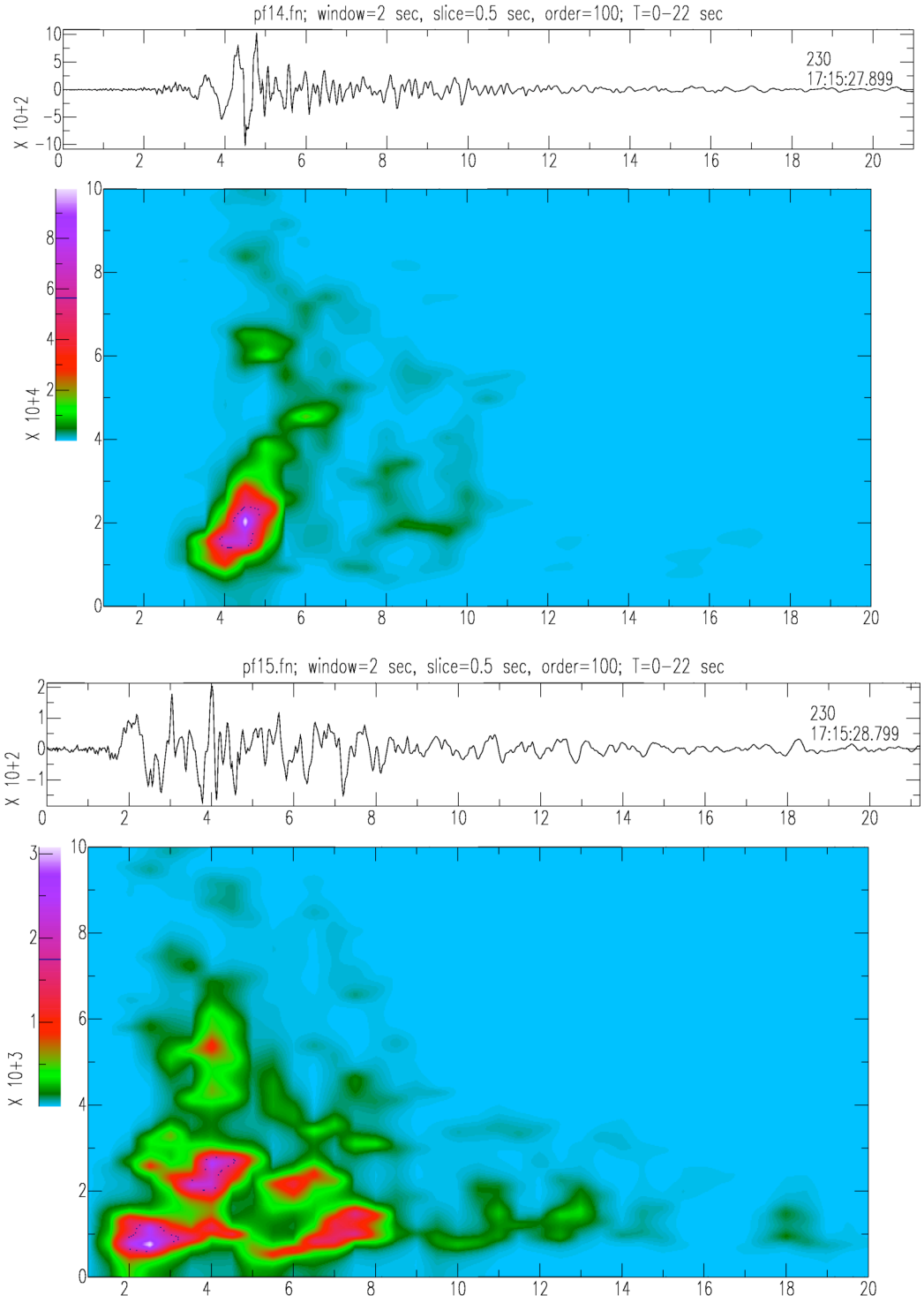

Figure 2. Time histories and spectrograms of recorded acceleration at stations PF14 (top panel) and PF15 (bottom panel). Acceleration unit is cm/s. Horizontal axis represents time in sec., and vertical axis of the spectrograms represents frequency in Hz. Color vertical scale corresponds to acceleration spectral amplitudes. Note that the peak spectral acceleration at PF14 is 30 times higher than that at PF15.

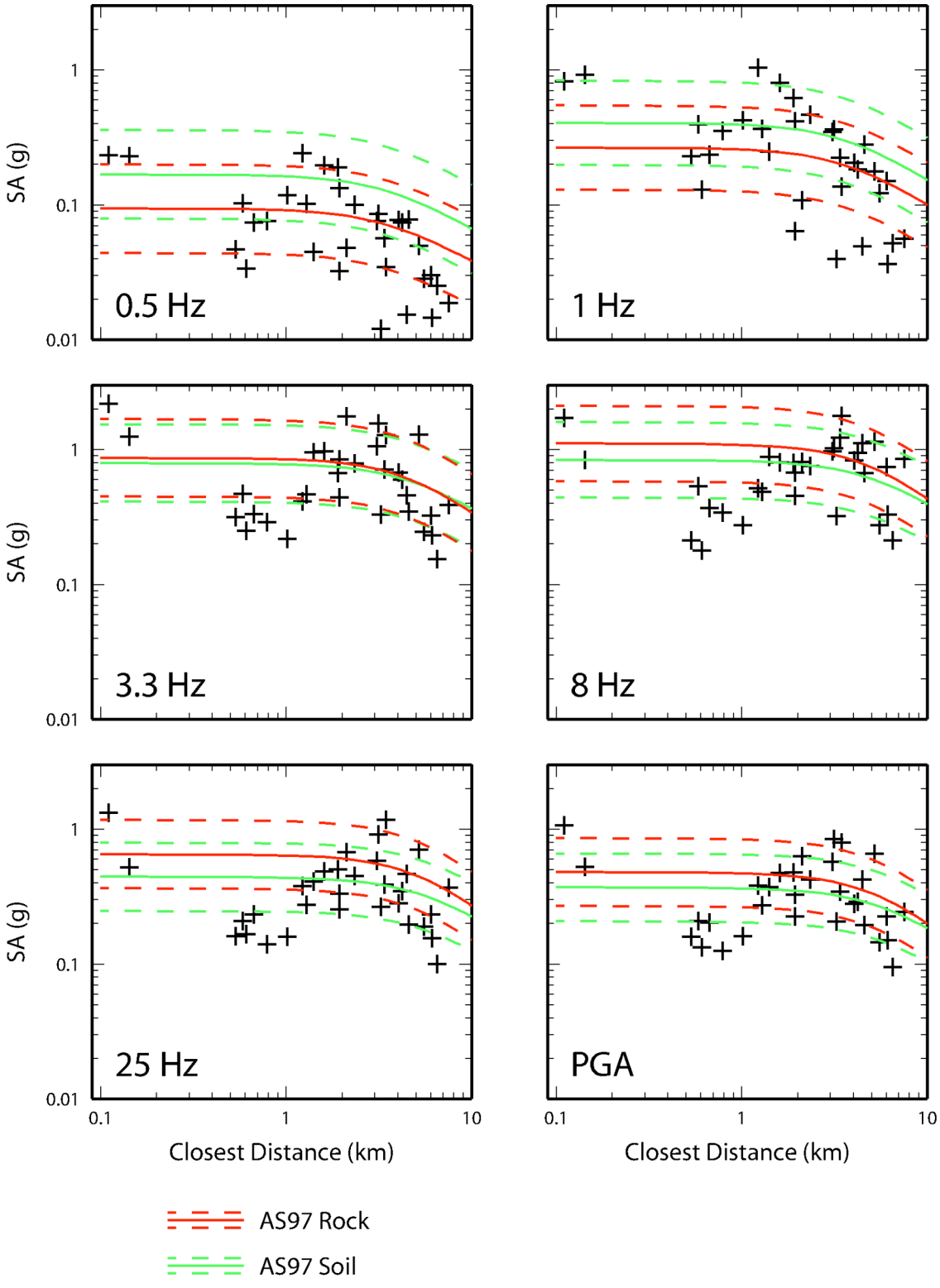

Figure 3a. Comparison of recorded spectral acceleration (crosses) and the Abrahamson and Silva (1997) empirical attenuation model for fault normal component.

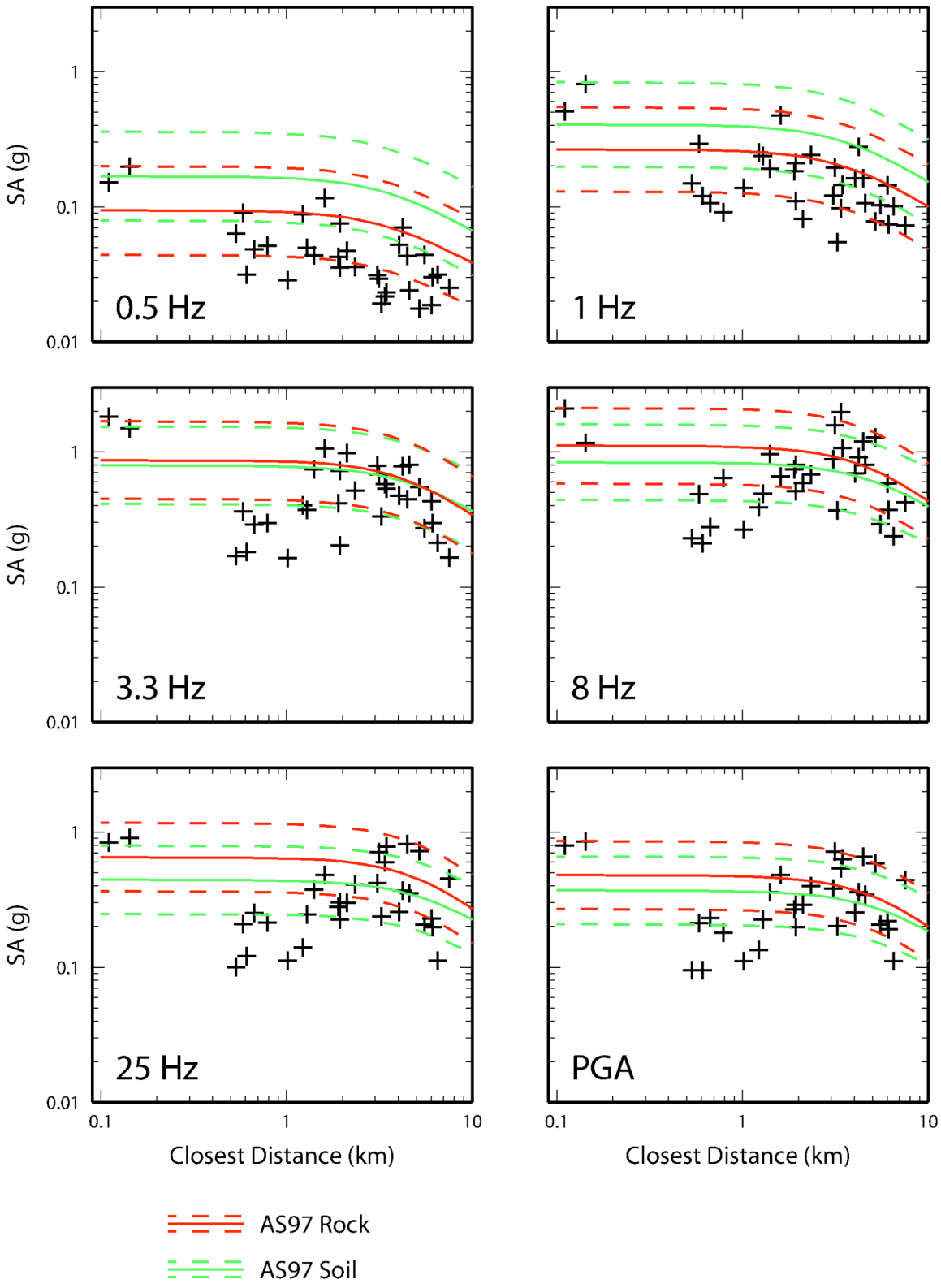

Figure 3b. Comparison of recorded spectral acceleration (crosses) and the Abrahamson and Silva (1997) empirical attenuation model for fault parallel component.

The site amplification at stations PF14 and PF16 is independent from the source type and location. This clear property also suggests that during the 2004 Parkfield earthquake the ground motion recorded at stations PF14 and PF16 was largely amplified by local site effects.

Clear trends in the amplification factors that also reflect site and local wave propagation effects are the followings:

1. The amplification observed at sites located in the fault zone is confined at frequencies 1Hz and lower. The amplification is more pronounced at sites located in both ends of the fault. Note that 1Hz falls in the frequency range where also the directivity effect is expected to amplify the fault-normal component of ground motion for this type of earthquake. At most of the sites located within 1km from the fault, fault zone and site effects deamplified the ground motion acceleration, and amplified the ground motion velocity.
2. At stations near the southern end of the fault, where the ground motion was relatively high, high frequency site effects are negligible.

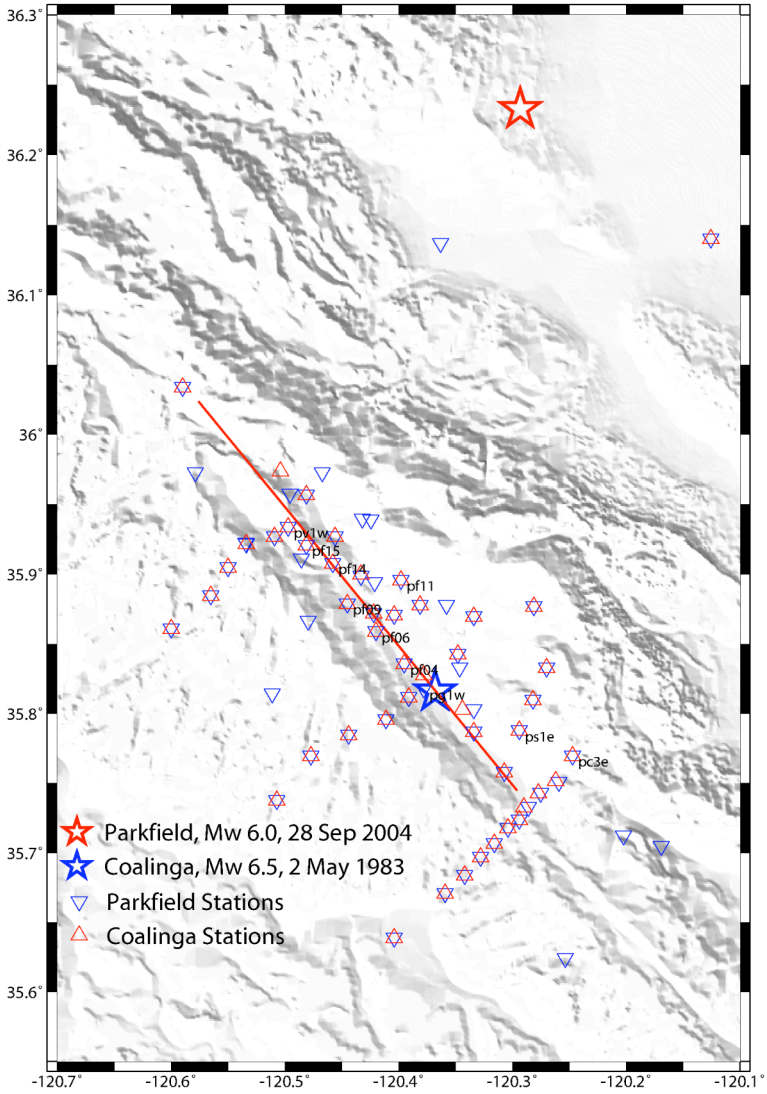

Figure 4. Map of the Parkfield area showing the location of the stations that recorded 2004 Parkfield earthquake (blue triangles) and 1983 Coalinga earthquake (red triangles). Also shown are the epicenter of the 2004 Parkfield earthquake (blue star) and the epicenter of the Coalinga earthquake (red star).

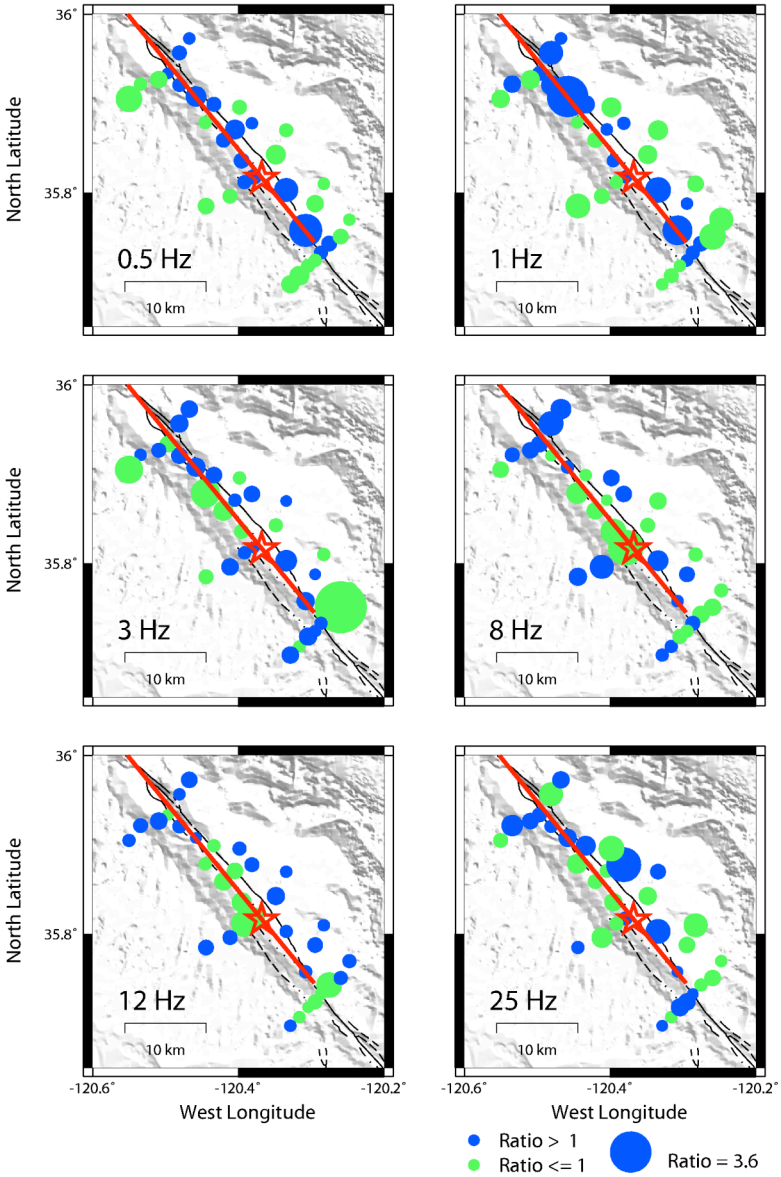

Figure 5. Site effect amplification factors estimated at stations that recorded the 1983 Coalinga earthquake. The circle's radius is proportional to the amplification factor. Blue circles indicate amplification and green circles indicate deamplification. Note that the largest amplification of 3.6 was observed at 1Hz at station PF14 which also recorded the highest acceleration during the 2004 Parkfield earthquake

RUPTURE KINEMATICS

Inversion Method

Our fault rupture kinemtics inversion method is similar to the one proposed by Hartzell and Heaton (1983). We set up the rupture plane as single fault plane with a strike angle of 140.8^{o} and dip angle of 89^{o} (Thurber et al., 2006). The length of the fault plane is 35 km and the width 16 km. The depth to the top of the fault is 0.1 km. In our inversion we used ground motion data recorded at stations with the fault distance smaller than 30 km. We excluded most of the stations with fault distance less than 1 km. These stations were excluded for several reasons. First, with our current representation of the fault surface by a single plane, stations that are very close to the fault may project on the wrong side of the

assumed fault plane. Second, the 1D Green's functions generated at these stations misrepresent the actual 3D effects of the structural heterogeneities of the fault zone.

The original acceleration data used in the inversion were integrated to velocity and band-pass filtered at 0.1-1 Hz. Two 1D regional velocity models were used to calculate Green's functions for sites located on the east and west sides of the fault, respectively (Thurber et al., 2003). The two models differ from each other in the top 10 km, with the west side model being 20% faster in the top 10 km. Since we inverted relatively high frequency ground motion velocity the 1D Green's functions were also corrected for local site effects using site-specific amplification factors. Several stations used in the inversion did not record the 1983 Coalinga earthquake. Consequently we were unable to use our site amplification factors obtained from recordings of the Coalinga earthquake to correct the synthetic Green's functions. Instead we used empirical site amplification factors derived using the empirical relations of Borcherdt (1994) and V_S^{30} value (e.g., Graves and Pitarka, 2004). Although very simplistic, the correction improves the quality of the slip inversion. In our trial inversions we varied the maximum rupture velocity between 2.5 and 3.5 km/s, but found that 3.0 km/s gave the best waveform fit. We used 20 time widows with duration of 0.8 sec and superposed by 0.4 sec.

Kinematic Rupture Model

Figure 6 shows the distributions of the final slip, and slip vector on the fault plane. Figure 7 shows contour lines of the rupture initiation time. The waveform fit for selected stations used in the inversion is shown in Figure 8. In our model the slip is concentrated in two large areas that occupy about 30% of the fault. The maximum slip of 40 cm is observed in a shallow slip area in the northern part of the fault. The average rake angle is 180 degrees. It indicates that this event was predominantly right-lateral strike slip. The total moment amounts to 1.53×10^{25} dyne.cm, corresponding to a moment magnitude of 6.1.

The only region with substantial shallow slip is in the northern part of the fault. Elsewhere the slip is relatively deep. The patch of slip in the southern edge of the fault seems to be controlled by the large ground motion observed at nearby stations. Although not well resolved, because of its proximity to the fault boundary, the slip in the southern part of the fault indicates that the fault rupture propagated bilaterally. The rupture gradually came to a stop in the northern end of the fault as opposed to an abrupt stop in the south where our kinematic model shows that the rupture speed was supershear for a short distance. The quick rupture arrest in the south suggests that the southern boundary between the Parkfield fault segment and the locked segment of the San Andreas fault is marked by a strong barrier.

In the north the shallow slip and rupture directivity affected the ground motion significantly. Combined with local site effects these source effects caused ground motion amplification at several sites located near the north end of the fault (e.g. PF14 and PF16). In contrast, in the south at stations PS1E and PC3E neither site effects nor rupture directivity were strong enough to be considered key factors in affecting the ground motion amplitude. In fact most of the stations in this area recorded relatively weak motion. It is possible that the larger ground motions observed at stations PS1E and PC3E were caused by the large amplitude shock wave created when the rupture in the southern part of the fault went supershear.

RUPTURE DYNAMICS

Our procedure for obtaining the dynamic rupture model of the earthquake is similar to the inversion procedure proposed by Dalguer (2002). His procedure is based on a trial-and-error technique in which the spatial distribution of the dynamic rupture parameters are obtained by step-by-step modifications that improve both the waveform fit between the recorded and calculated data, and the fit between the kinematic and dynamic final slip and initial rupture time (e.g. Pitarka and Dalguer, 2003; Pitarka, 2005). The stress time history on the fault is calculated using a 3D finite-difference method (Pitarka and Dalguer,2003). Our method of modeling spontaneous rupture uses the so-called "inelastic fault

zone" formulation proposed by Dalguer and Day (2004). The rupture process is controlled by a simple slip weakening law as proposed by Andrews (1976). The stress time history is then used to estimate dynamic rupture parameters such as dynamic stress drop, static stress drop, and strength excess.

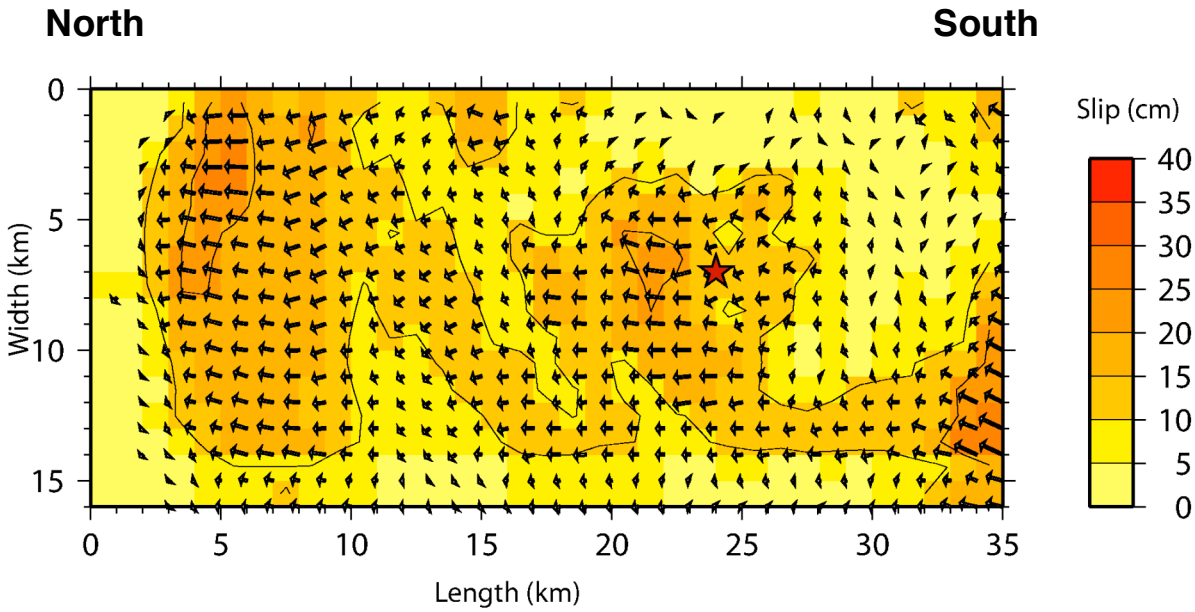

Figure 6. Total slip and final slip vector distribution for the kinematic rupture model of the 2004 Parkfield earthquake obtained by inverting near-fault ground motion velocity in the frequency range 0.01-1.0 Hz.

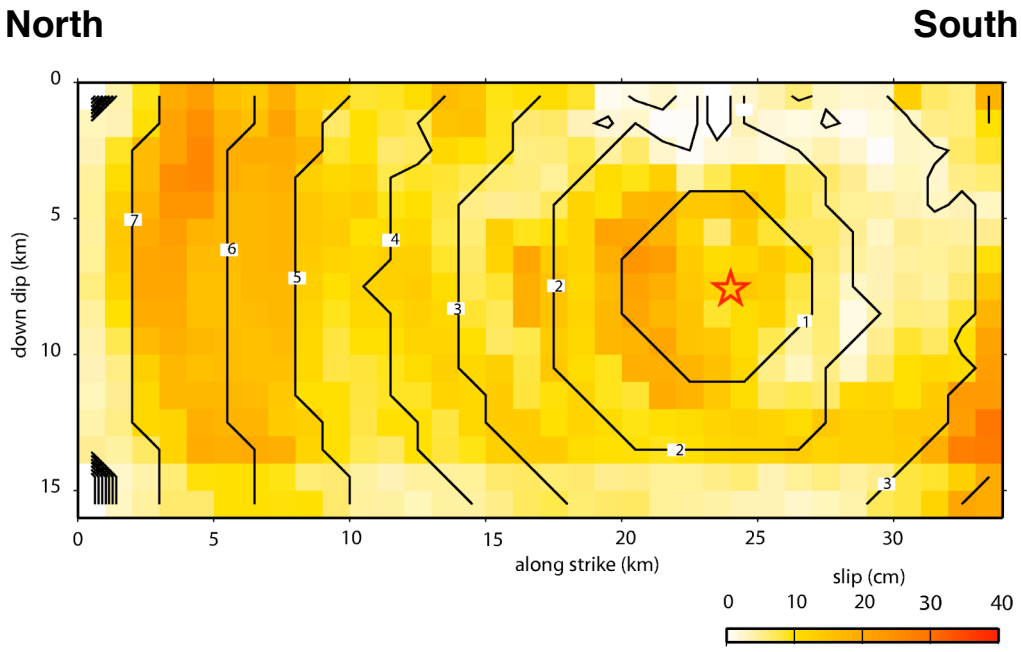

Figure 7. Contour lines of rupture time initiation for the kinematic rupture model of the 2004 Parkfield earthquake

Figure 8. Comparison of recorded (black) and synthetic ground motion velocity (red) calculated with the kinematic model at CGS and USGS stations shown in the upper panel and lower panel, respectively.

In order to initiate the dynamic rupture inversion procedure we used the spatial distribution of the slip time history on the fault derived from the kinematic rupture model obtained by Liu et al. (2006). We did not use our kinematic slip model since the slip time history obtained with our multiple-time window inversion technique is given by overlapping ramp functions. This type of representation of the slip time history can cause numerical noise when used to model fault boundary conditions with numerical methods. In the non-linear inversion performed by Liu et al. (2006) the smooth slip time history is appropriate for finite-difference rupture propagation modeling. The fault location and its geometry adopted in their study are similar to those used in our kinemtic inversion. In the spontaneous rupture modeling we assumed that the fault slipped with a rake angle of 180 degrees. The preferred dynamic fault rupture model is shown in Figure 9. The dynamic rupture model suggests that the average stress drop during the earthquake was very low, less than 2 MPa. Elevated stress drops of about 5-10 MPa are concentrated in several small areas throughout the fault. Because of their relatively high stress drop, these areas of energy bursts can generate near-fault ground motion with locally large acceleration. The strength excess, which is one of the factors that controls the fracture energy, was low throughout the fault, except for the southern part where combined effects of high strength excess and low dynamic stress drop have caused the rupture to quickly stop. The rupture speed seems to have been larger than the shear-wave speed around the hypocenter and along a small portion of the southern end of the fault.

DISCUSSION AND CONCLUSIONS

The unprecedented relatively dense ground motion recordings of the 2004 M_w6 Parkfield earthquake demonstrated that near-fault ground motion of shallow strike-slip earthquakes can be extremely variable. The degree of variability for this earthquake was related more to site conditions, including fault zone effects, rather than source effects. The observation of alternated very low and very high ground motion at many sites located close to the fault, and our investigation of site effects support this conclusion.

Our study cannot give a definitive answer to the question of how much the rupture process was responsible for the localized but very high acceleration observed near the fault. Unfortunately due to the numerical requirement, our kinematic and dynamic rupture models cannot resolve the process of generation and propagation of ground motion energy at frequencies higher than 1Hz. Nevertheless they indicate that in a small area near the north end of the fault the shallow asperity with relatively large stress drop caused increased level ground motion. Also in its south end a small portion of the fault ruptured with supershear speed. The elevated ground motion observed in this area (stations PS1E and PC3E) was probably due to the shock wave generated locally as a result of the supershear rupture. This is a speculation that needs further investigations of the source process using higher resolution 3D modeling. The results of our investigation of site effects support the hypothesis that the very large ground motion at station PF14 which recorded the highest acceleration of 1.3g, was mostly due to site effects.

Our study leaves open the discussion about the possibility that a part of the spatial variation of high frequency ground motion was generated by very small asperities with large stress drop and high slip velocity. The difference between the observed fault-normal and fault parallel motion, which is an indication of rupture directivity effects, shows that near-fault ground motion from strike-slip earthquakes of moderate magnitude, such as the 2004 Parkfield earthquake, can be affected by the rupture directivity even at frequencies as high as 3 Hz.

Given the complexity in the observed ground motion and the band-limited information on the source process obtained for this earthquake it is interesting to see how well our broad-band numerical simulation techniques perform in terms of predicting the average ground motion, the maximum ground motion and spatial variation of peak acceleration.

We simulated the acceleration time history up to 10 Hz at all near-fault stations. In the simulation we used the technique of Graves and Pitarka (2004) and the kinematic rupture model presented here. The simulation technique combines deterministic and stochastic approaches to model the low frequency and high frequency parts of the acceleration time history. The simulated acceleration was finally corrected for site effects using site category and V_S^{30} values obtained from Wills et al. (2000). Figure 10 shows the goodness of fit between the simulated and recorded ground motion. In general the spectral acceleration is matched very well at all considered periods. A negligible bias is observed. In Figure 11 we have plotted the recorded and simulated peak spectral acceleration as a function of distance at several periods, and compared it with the corresponding attenuation model of Abrahamson and Silva (1997). The comparison shows that on average the ground motion from the 2004 Parkfield earthquake follows the existing empirical attenuation model. The simulation fails to produce the observed near-fault spatial variation of spectral acceleration. This is not surprising since, because due to lack of information about the local underground structure at all strong motion sites, our simulation was mostly driven by the source process. Our study suggests that in order to capture wave propagation effects due to fault zone structure and local site conditions, 3D Green's functions and site specific corrections based on direct measurements of velocity are needed. Applying site-specific corrections, derived from the 1983 Coalinga earthquake data, instead of empirical site corrections, to simulated peak acceleration and peak velocity results in a more favorable comparison between recorded and simulated peak acceleration and peak velocity (shown in Figure 12), especially in the area north of epicenter.

The main conclusion of this study is that the relatively high and low peak acceleration, and the spatially variable near-fault ground motion observed during the 2004 Parkfield earthquake were mostly caused by local wave propagation and site effects. Unless such site effects are known, the broad-band strong motion simulation can not reproduce the ground motion variability very well. On the other hand our strong ground motion simulation technique yields good results in predicting the spatial ground motion distribution since it allows for realistic representation of the source process, underground structure, and local site effects.

AKNOWLEDGEMENTS

The authors would like to thank Anthony Shakal and Hamid Haddadi for many helpful discussions. This research was supported by the California Strong Motion Instrumentation Program.

REFERENCES

Abrahamson,N.A. and Silva W.J. Silva." Empirical response spectral attenuation relations for shallow crustal earthquakes", Seismological Res. Letters, 68,94-127,1997

Andrews,D.J." Rupture velocity of plane-strain shear cracks", J.Geoph. Res., 81, 5679-5687,1976

Borcherdt, R. "Estimates of site-dependent response spectra for design (methodology and justification)", Earthquake Spectra,10(4),617-653, 1994

Dickinson, W.R. "Structural relations of San Andreas fault system, Cholame Valley and Castle Mountain Range, California", Geological Society of America Bulletin, 77, 707-725, 1996

Dalguer L. "Strong motion prediction based on dynamic fault modeling", 2002 Report on MEXT Project, 2002

Dalguer, L.A. and Day S.M. "Split nodes and fault zone models for dynamic rupture simulations", EOS Trans. AGU, 85(47), Fall Meet.Supl. Abstract S41A-0944, 2004

Eberhart-Philips,D., and Michael A.J. "Three-dimensional velocity structure, seismicity,and fault structure in the Parkfield Region, central California", Journal of Geophysical Research,98,15,737, 1993

Graves, R. and Pitarka A. "Broadband time history simulation using a hybrid approach", Proceedings of the 13th World Conference on Earthquake Engineering, Vancouver, Canada, August 1-6, 2004, Paper No. 1098, 2004.

Haddadi,H.,Shakal A.,.Kalkan E.and Roffers P. “On the strong ground shaking at the Fault Zone 16 and nearby ststions of Parkfield array” Seism.Res.Lett.,77,244, 2006

Hardebeck, J.L., and A.J. Michael A.J., “Earthquake locations before and after the 2004 M6.0 Parkfield earthquake”, AGU Fall Meeting Abstracts, 85 (47), 2004.

Hartzell , S.H., and Heaton T.H. “Inversion of strong ground motion and teleseismic wavefor data for the fault rupture history of the 1979 Imperial Valley, California earthquake”, Bull.Seism.Soc.Am. 73, 1553-1583, 1983.

Langbein,J., Borcherdt R., Dreger D., Fletcher J., Hardebeck J.L., Hellweg M., Ji C., Johnston M.,Muray J.R., and Nadeau R. “Preliminary report on the 28 September 2004, M6.0 Parkfield, California earthquake”, Seismological Res.Lett., 76,10-26, 2005

Liu, P., Custodio S. and Archuleta R.J.(2006). “Kinematic inversion of the 2006 M_w6.0 Parkfield earthquake including site effects:, Bull. Seism.Soc.Am. (in press), 2006

Li,Y-G.,Chen P., Cochran E.S.,Vidale J.E., and Burdette T. “Seismic evidence for rock damage and healing on the San Andreas fault associated with the 2004 M6 Parkfield earthquake”, Bull. Seism.Soc.Am. (in press), 2006.

Peng,Z.,Y. Ben-Zion,A. Michael, Zhu L. “Quantitative analyses of seismic fault zone waves in the rupture zone of the 1992 Landesr, California, earthquake:evidence for shallow trapping structure”, Geophys.J.Int. 155,1021-1041,2003.

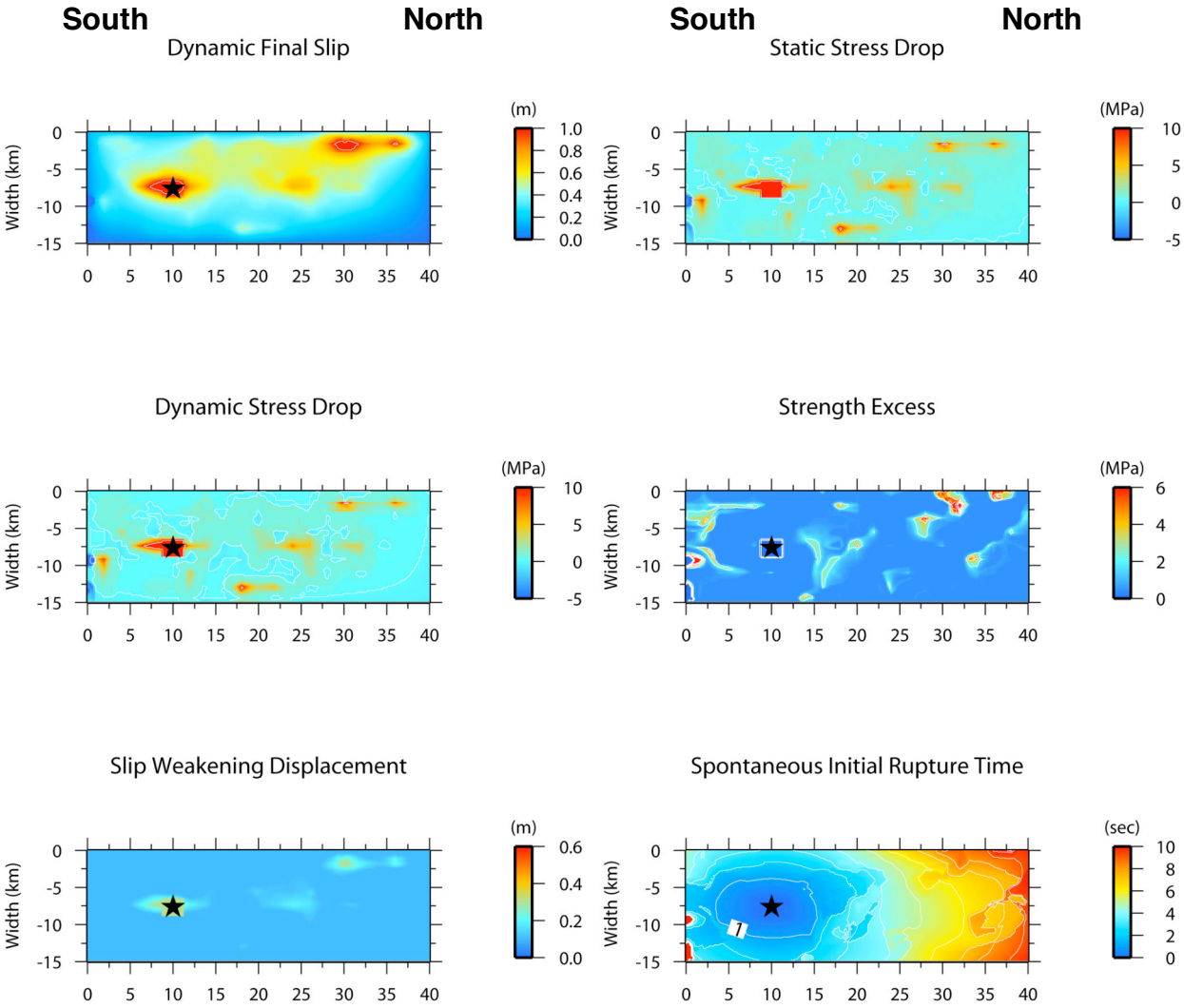

Figure 9. Dynamic rupture model of the 2004 Parkfield earthquake obtained by a trial-and-error inversion scheme and spontaneous rupture modeling. Star indicates the rupture initiation point.

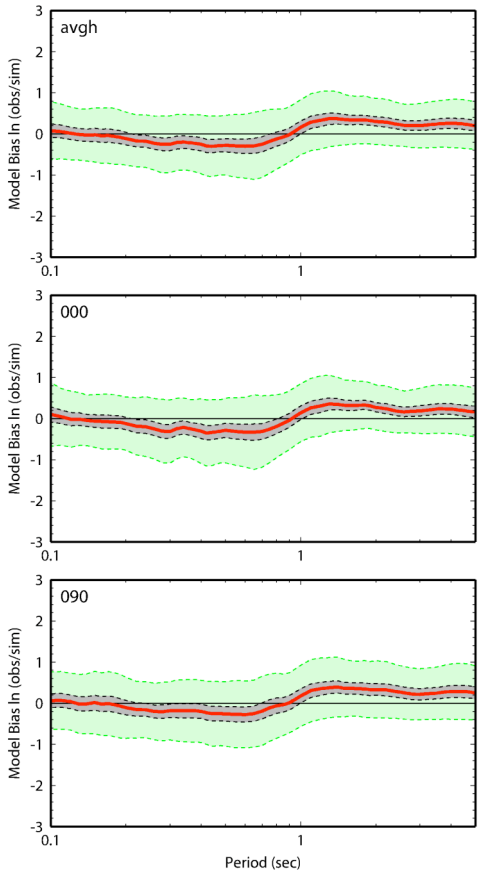

Figure 10. Spectral acceleration goodness-of-fit computed for the average of horizontal components (top panel), fault parallel component (middle panel), and fault-normal component (bottom panel). Red line plots mean model bias averaged over all sites. Gray shading denotes 90% confidence interval of the mean and green shading denotes interval of one standard deviation.

Pitarka, A. "3D elastic finite-difference modeling of seismic motion using staggered grids with nonuniform spacing", Bull.Seism.Soc.Am. 89, 54-68, 1999.

Pitarka A., and Dalguer L.A. "Estimation of dynamic stress parameters of the 1992 Landers earthquake", EOS Trans.AGU, 84(46). Fall Meeting Supp. Abstract. S52A-0109, 2003.

Pitarka A. "Rupture dynamics of the 1989 Loma Prieta earthquake" , Seismolocal Research Letters, Vol 76, Nr.2., 252,2005

Shakal, A., Graizer V., Huang M., Haddadi H., and Lin K. " Strong-motion data from the M6.0 Parkfield earthquake of September 28,2004", Proceedings of SMIP05 Seminar on Utilization of Strong Motion Data, Los Angeles, CA, 1-18,2005.

Thurber,C., Roecker S.,Roberts S.K.,Gold M.,Powell L.,and Rittger K." Earthquake locations and three-dimensional fault zone structure along he creeping section of the San Andreas fault near Parkfield, CA": Preparing for SAFOD. Geophys.Res.Lett. 3, 1112, doi: 10.1029/2002GL016004, 2003

Wills,C., Petersen, M.,Brayant,W.,Reichle, M.,Saucedo, G.,Tan,S.,Taylor,G.,Treiman,J. "A site condition map for California based on geology and shear-wave velocity", Bull.Seism.Soc.Am. 90,6B, S187-S208, 2000.

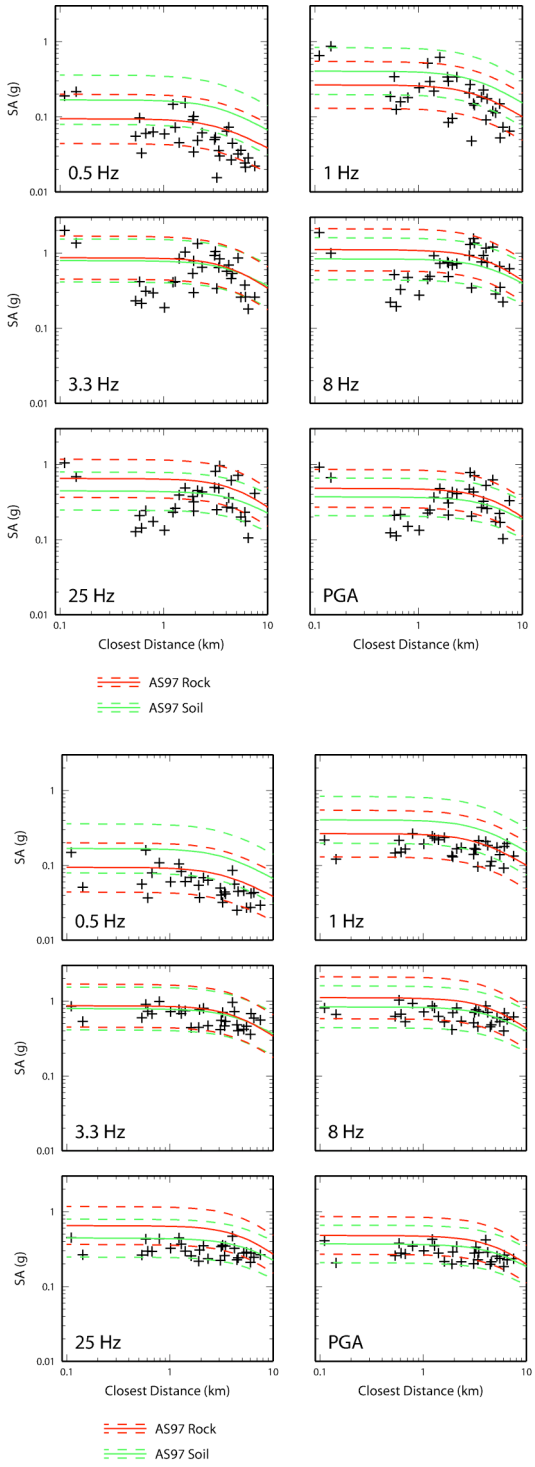

Figure 11. Comparison of empirical attenuation models of horizontal spectral acceleration for rock (red lines) and soil (green lines) with recorded (top panels) and simulated (bottom panels) spectral acceleration for the 2004 Parkfield earthquake. Crosses indicate spectral acceleration. The empirical attenuation model is taken from Abrahamson and Silva (1997) .

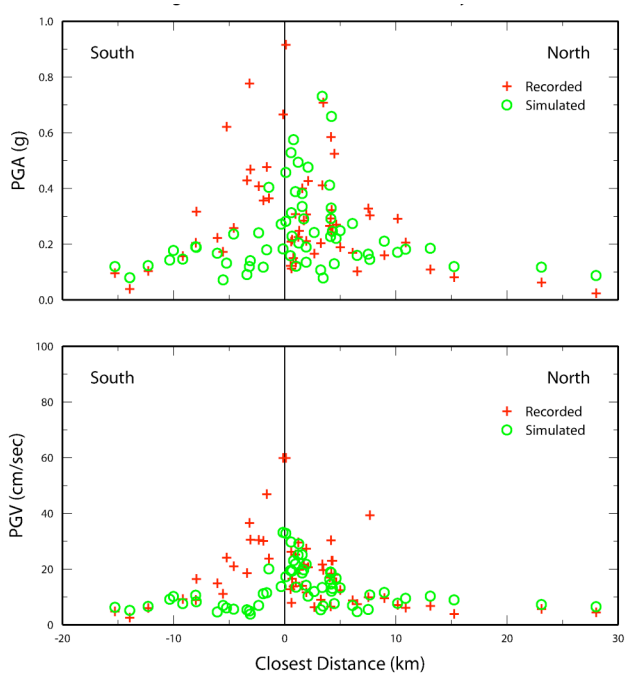

Figure 12. Comparison of recorded (crosses) and simulated (circles) peak ground acceleration and peak ground velocity. The simulated values include site corrections. At sites that recorded the Coalinga earthquake the site correction was derived from the analyzes of weak motion data recorded during the Coalinga earthquake.